Lab on a Chip

Acoustic bubble for spheroid trapping, rotation, and culture: a Tumor-on-a-Chip platform (ABSTRACT platform)

Journal:	*Lab on a Chip*
Manuscript ID	LC-ART-11-2021-001012.R1
Article Type:	Paper
Date Submitted by the Author:	21-Dec-2021
Complete List of Authors:	Gao, Yuan; University of Illinois at Chicago, Mechanical and Industrial Engineering Wu, Mengren; University of Illinois at Chicago Luan, Qiyue; University of Illinois at Chicago, Biomedical Engineering Papautsky, Ian; University of Illinois at Chicago, Bioengineering Xu, Jie; University of Illinois at Chicago, ;

Lab on a Chip

ARTICLE

Acoustic bubble for spheroid trapping, rotation, and culture: a Tumor-on-a-Chip platform (ABSTRACT platform)

Received 00th January 20xx,
Accepted 00th January 20xx

DOI: 10.1039/x0xx00000x

Yuan Gao,[a] Mengren Wu,[a] Qiyue Luan,[b] Ian Papautsky,[b] and Jie Xu*[a]

Cancer is the leading cause of death globally, with 90% of deaths being caused by cancer metastasis. Circulating tumor cells (CTCs) play an important role in early diagnosis of cancer metastasis and in monitoring of therapeutic response. Therefore, reliable methods to isolate, collect and culture CTCs are required to obtain information on metastasis status and therapeutic treatment. In this work, we present a CTC-processing system: acoustic bubble for spheroid trapping, rotation, and culture: a Tumor-on-a-Chip platform (ABSTRACT). The platform consists of a main channel, several parallel sub-microchannels with microcavities and culture chambers. The microcavity is designed to trap a bubble with desired shape at the entrance of the sub-microchannel. Under the acoustic actuation, the trapped bubble oscillates and creates a secondary radiation force to trap and rotate CTCs at a desired location. By controlling the acoustic bubble, CTCs can be continuously trapped from the blood flow, rotated to form a spheroid, and released to the microchamber for culture. We systematically investigated the effects of device geometry, flow parameters, and input voltage on trapping of CTCs to optimize the performance. Additionally, the successful on-chip spheroid culture demonstrates the biocompatibility and the simplicity of this platform. Besides simplifying conventional complex CTC processing procedures, this ABSTRACT platform also shows great potential for downstream analysis of tumor cells, such as monitoring the progression of metastasis and personalized drug testing.

1. Introduction

As reported by World Health Organization (WHO), cancer is a leading cause of death globally (~10 million deaths in 2020), with 90% of deaths being caused by cancer metastasis.[1, 2] The main reason for causing cancer metastasis is circulating tumor cells (CTCs), which are tumor cells derived from primary tumors and circulate in the bloodstream and lymphatic system. Therefore, CTCs play an important role in early diagnosis of cancer metastasis and in monitoring of therapeutic response. Compared with conventional invasive biopsy methods, isolating CTCs from patient blood provides a less invasive approach, termed “liquid biopsy”, for early cancer diagnosis and future therapies.[3] However, due to the rarity in blood, CTCs isolation, collection and characterization are technically challenging. Many macro-scale CTCs isolation methods have been developed based on physical properties and biological characteristics, including size-based filtration, density-based centrifugation, and immunocapture.[4] Although these methods enable isolating CTCs with high throughput, they normally suffer from several limitations such as low cell viability, lack of automation, and low capture efficiency.[5]

In recent years, microfluidics has attracted great interest in isolation and downstream analysis of CTCs on the microscale because of their low sample volume requirements, high controllability and biocompatibility. Based on different physical characteristics, CTCs have been isolated from blood in microfluidic devices with the use of various physical principles. For instance, utilizing the hydrodynamic methods, such as deterministic lateral displacement (DLD), dean flow fractionation (DFF), and microvortex, researchers have successfully separated CTCs from blood with high throughput.[6-9] By applying magnetic force, CTCs tagged with magnetic beads have been isolated with high isolation capacity on a microfluidic chip.[10] Based on the difference of size and dielectric properties between circulating tumor cells (CTCs) and blood cells, dielectrophoresis has been applied for isolating CTCs from blood.[11] Acoustofluidic methods have also been explored to separate CTCs with the advantages of contactless, label-free and easy to integrate with other microfluidic techniques. Actuated by surface acoustic waves (SAWs) and bulk acoustic waves (BAWs), CTCs have been efficiently isolated from blood samples.[12-14] After isolation from blood samples, CTCs collection and *in vitro* CTC culture are important steps for downstream characterization.[15] The aforementioned microfluidic techniques offer advantages in separating CTCs. However, releasing CTCs from the collection substrate for CTC cultures presents challenges. Therefore, an effective “all-in-one” approach to trapping, release and culture CTCs is highly sought after, which would greatly facilitate analysis like mutation profiling and drug

[a] Department of Mechanical and Industrial Engineering, University of Illinois at Chicago, IL 60607, USA. E-mail: jiexu@uic.edu
[b] Department of Biomedical Engineering, University of Illinois at Chicago, Chicago, IL 60607, USA

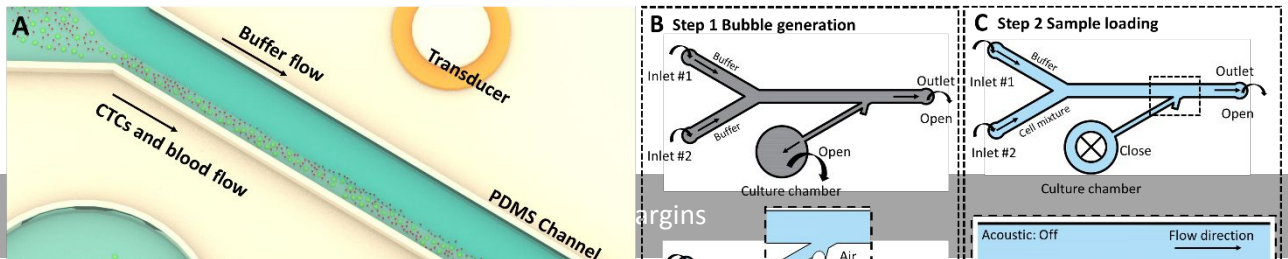

screening, and provide critical information for personalized medicine for cancer treatment.[15]

As an emerging tool in fluids and cell manipulation, acoustic bubbles in microfluidics show the possibility to address the challenges above.[16, 17] In low-frequency acoustic fields, bubbles can be remotely excited to act as pumps,[18, 19] mixers,[20, 21] switches,[22] sorters[14, 23] and transporters[24] in various lab-on-a-chip (LOC) applications. Acoustic bubbles can generate secondary radiation force (SRF) on cells at a specific frequency range, which could be harnessed to trap and rotate cells on the bubble surface when the radiation force exceeds the external drag forces.[25] Since the amount of SRF depends on the size and density of the cells or particles, acoustic bubbles can be used to selectively capture cells or microparticles. In microfluidic devices, the location of the bubbles can be precisely controlled by both active and passive methods, making it possible to trap cells and particles in desired locations.[17] Additionally, it is shown that the acoustic bubble is biocompatible in manipulating tumor cells and microorganisms, which could help maintain cell viability.[26, 27] These above advantages make the acoustic bubble a promising candidate for CTC-processing.

In this article, we present an effective approach—acoustic bubble for trapping, rotation and culture CTC spheroid on a Tumor-on-a-Chip platform (ABSTRACT). By creating microcavity structures, air bubbles can be passively trapped in the designed polydimethylsiloxane (PDMS) microchannel with desired shape, size and location. With the control of acoustic excitation, the bubbles can trap the CTCs from the spiked blood flow in the main channel, form the CTC spheroids and then release them to the sub-channels for culture and observation. During the culture process, this ABSTRACT platform enables delivering of the culture medium from the main channel to the sub-channels and culture chambers. In this work, we also varied parameters including microcavity dimensions, flow rates and sheath flow ratios to optimize the trapping efficiency of the ABSTRACT platform. With the growing interest of CTC processing in microfluidics, our approach provides a convenient, simple, and effective way to integrate multi-step CTC-processing procedures on one chip.

2. Materials and methods

2.1. Device fabrication

In this work, the polydimethylsiloxane (PDMS) microchannel with the cavity structures was fabricated using soft lithography and mold replica technique. In the fabrication process, the silicon master mold was fabricated by spin-coating SU-8 2050 photoresist, UV exposure and development. A mixture of PDMS (Sylgard 184, Dow Corning) was then prepared with 10:1 (w/w) base to curing agent ratio and placed in a vacuum desiccator (Bel-Art Scienceware, NJ) for degassing. After that, the PDMS mixture was poured on the silicon master mold and then cured in the oven at 65 °C for 1 h. Once the PDMS microchannel layer was cured, it was peeled off gently and punched to form the inlet, outlet and culture chamber for loading and collecting samples. Afterward, the PDMS microchannel layer was bonded with a glass microscope slide (75 mm × 50 mm × 0.90–1.10 mm, Corning®, USA) by oxygen plasma treatment for 1.5 min. Finally, a piezoelectric transducer with a resonant frequency of 4 kHz (Vktech, USA) adhered to this glass slice covered by plastic double-sided adhesive tapes (Adhesives Research, Glen Rock, PA).

2.2. Experimental setup

To create acoustic waves and activate the ABSTRACT platform, the piezoelectric transducer was driven by square wave signals from a function generator (DG1022U; Rigol Technologies Inc., Beijing, China) and amplified by a voltage amplifier (Tegam 2350, Tegam Inc., Madison, OH). After that, the platform was mounted on the stage of an inverted microscope (Nikon Eclipse Ti-S, Nikon Instrument Inc), equipped with a high-speed camera (Phantom Miro M310, Vision Research Inc., USA) for observing and recording the motion of the CTCs in the microchannel.

During the experiment, to characterize the performance of this device, we studied the effect of the device parameters, flow parameters and acoustic parameters applied on bubbles. For the device parameters, cavity structures with different angles (45°, 60°, 90°, 120°, 135°) were set for evaluating the performance of the device, while the width and the height of the microchannel and the cavity structure were fixed (main channel: 500 μm × 100 μm (width × height), sub-channels: 200 μm × 100 μm (width × height), microcavity structures: 200 μm × 100 μm (width × height)). For the flow parameters, different flow rates (1, 2, 3, 4 μl/min) and different sheath flow ratios (1:0, 1:1 and 1:5) were set for experiments. To adjust the blood flow rate and flow ratio in the microchannel, buffer flow and blood flow were injected into two inlets and controlled by two syringe pumps. Different input voltages were also applied for

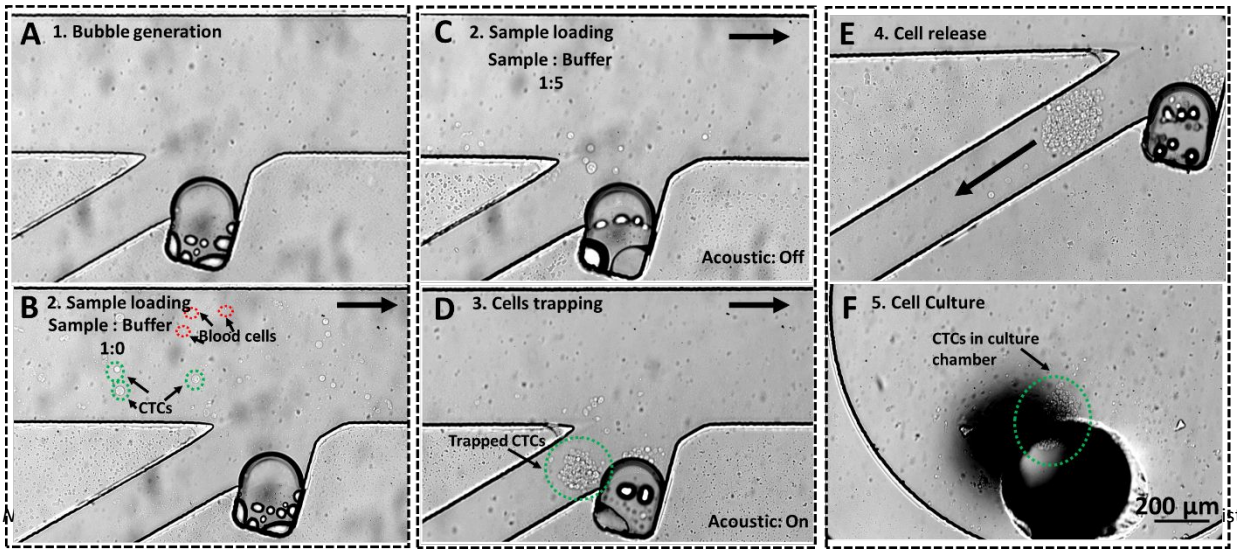

Figure 2. Experimental demonstration of CTC-processing in the acoustic bubble-based Tumor-on-a-Chip platform. (a) An air bubble was created when liquid flows through the channel. (b), (c) After the bubble was generated in the cavity structure, the sample was loaded with different sheath flow ratios (1:0,1:5). (d) CTCs were trapped and rotated under acoustic actuation to form the spheroid. (e) The spheroid was loaded into the culture chamber when the acoustic was off. (f) The spheroid entered the culture chamber for culture.

exploring the influence of acoustic amplitude on trapping efficiency.

2.3. Sample preparation

Fresh porcine whole blood from Innovative Research Inc. (Novi, MI) were used in experiments, which were anticoagulated by heparin solution. To visualize the trapping effect, the diluted sample was applied for this study, which consists of 6.25% blood and 93.75% 1× PBS solution.

A549 lung cancer cells (CCL-185, ATCC, USA) used in experiments were cultured in RPMI 1640 Medium (Mod.) 1X with L-Glutamine (Corning, USA) supplemented with 10% (vol/vol) heat-inactivated FBS (GeminiBio, USA) and 1% (vol/vol) antibiotic–antimycotic (Invitrogen, USA) at 37°C, 5% CO_2 in a humidified incubator. A549 cell suspensions were made by dissociating cells with 0.25% trypsin–EDTA, centrifuging cells at 50g for 5 min, and re-suspending in growth media.

To prepare the samples for the experiment, the A549 lung cancer cells were spiked into the diluted porcine whole blood in the experiment (1×10^5 cancer cells/ml). The spiked blood sample was then processed with the ABSTRACT platform to investigate the effects of device geometry, flow parameters, and input voltage, as well as to demonstrate the spheroids collection and culture. While the concentration of the cancer cells of the spiked blood sample is higher than the typical concentration of clinical samples from patients, we use it as a baseline to allow for the demonstration and proof of concept of the device with more accurate quantification and characterization.

2.4. Spheroid culture and observation

Prior to the sample loading, the ABSTRACT platform was sterilized by exposure to the UV light for 30 min and then rinsed with 70% ethanol. To prevent spheroid adherence to the culture chamber, 0.5% (w/v) sterilized polyvinyl alcohol (PVA, Sigma Aldrich) solution in DI water was introduced in the microchamber and incubated for 60 min. After PVA solution was washed by PBS, the ABSTRACT platform was ready for loading samples.

After acoustic actuation, the spheroids were formed and collected into the culture chamber. During the culture process, the culture medium was delivered to the spheroids by diffusion and exchanged every 24 hr. Spheroid viability was monitored by an inverted fluorescence microscope (Olympus). The fluorescence-based live/dead cell viability assay was performed using a LIVE/DEAD™ Cell Imaging Kit (R37601, Invitrogen, Thermo Fisher Scientific) and the viability was measured by the software Image J (ratio of green fluorescence area over total spheroid area).

3. Results and discussion

3.1. Working mechanism of the ABSTRACT platform

A schematic illustration of the acoustic bubble-based Tumor-on-a-Chip platform for trapping, rotation and culture of CTC spheroids is shown in Figure 1. This ABSTRACT platform consists of a predesigned microchannel with a cavity structure and a piezoelectric transducer bonded to a glass substrate. The microchannel is filled with air before the liquid injection. When the liquid flows through the microchannel, the bubble is passively formed in the pre-designed sidewall cavity structure due to the surface tension and contact line pinning at the edge of the cavity.[28] The piezoelectric transducer can induce an acoustic field to actuate the bubble when an input voltage is applied. In a low-frequency acoustic field (23-28 kHz), the trapped air bubbles are actuated and induce two important phenomena — microstreaming flow induced drag force and secondary radiation force (SRF). Under the action of these two forces, CTCs are trapped on the bubble surface and separated from blood flow due to the difference in size and density. Besides trapping CTCs, the acoustic bubble also generates rotational motion for CTCs on its surface. With the help of the rotational motion, the CTCs aggregate and form a CTC spheroid. The size of the spheroid then increases with an increasing number of trapped CTCs. When the spheroid reaches the desired size, it is released to the culture chamber for on-chip

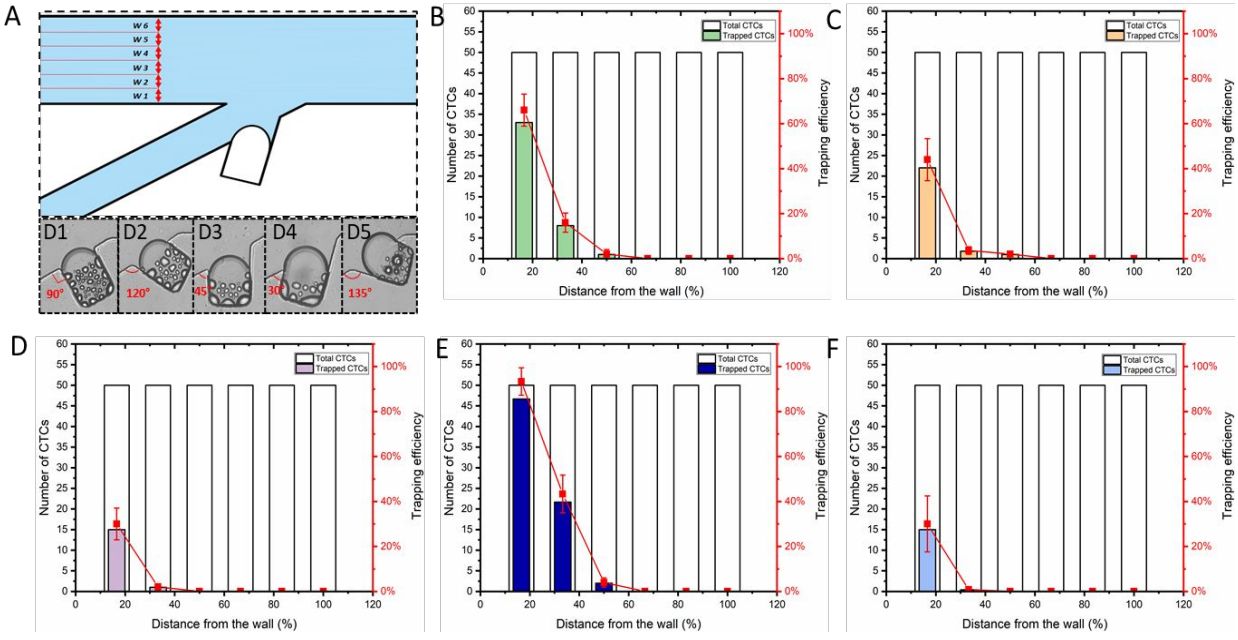

Figure 3. (a) Six regions are equally divided for measuring the sample distance from the wall. Different shaped bubbles are trapped in five angled cavity structures. (b)-(f) Effect of the cavity geometry (D1-D5) and sample distance from the wall on CTCs trapping efficiency. The data is presented as average ± standard deviation (n=3).

spheroid culture by turning off the acoustic field. During the culture process, the nutrient is delivered from the main channel to the chamber by diffusion.

The detailed trapping mechanism in this study is described as follows. When the air bubble is exposed to the acoustic field around its resonant frequency, it undergoes radial and translational oscillation and creates a circulating flow pattern, called microstreaming. In the microfluidic system, when CTCs and blood cells are suspended in microstreaming flow and laminar flow field, they experience a steady drag force, which can be described as[29]:

$$\boldsymbol{F_D} = 6\pi\mu r\boldsymbol{v} \quad (1)$$

$$\boldsymbol{v} = \boldsymbol{v_l} - \boldsymbol{v_p} \quad (2)$$

where r, μ, $\boldsymbol{v}$, present the radius of the cell, the viscosity of the fluid media and the relative velocity of the fluid ($\boldsymbol{v_l}$) and cell ($\boldsymbol{v_p}$), respectively. Another important force that acts on CTCs and blood cells, called secondary radiation force, is a time-averaged radiation force produced by the fluctuation of bubble volume induced scatter pressure field. This force is given as:

$$\boldsymbol{F_{SRF}} = 4\pi\rho_l \frac{\rho_l - \rho_p}{\rho_l + 2\rho_p} \frac{r^3 {r_b}^4}{d^5} \omega^2 \boldsymbol{\xi}^2 \quad (3)$$

where ρ_l, ρ_p are the density of the liquid and the cell, r_b is the radius of bubbles, d denotes the distance between the center of the bubble and the cell, ω presents the applied frequency, and ξ is the oscillation amplitude of the bubble[30]. From several theoretical and numerical studies, whether the movement of a cell is dominated by drag force or radiation force depends on the size, as well as the properties of the cell[31]. If the cell is dominated by microstreaming flow induced drag force, the cell continues to follow the microstreaming flow. On the other hand, if the cell is dominated by the secondary radiation force, the cell is trapped on the bubble surface. Therefore, CTCs are trapped on the bubble surface since the secondary radiation force is greater than the drag force, while most blood cells follow the streamline to the outlet because the drag force is dominant.

The CTC-processing steps in this ABSTRACT platform are shown in Figure 1 and Figure 2. When the culture chamber is opened, the buffer flow is injected from one inlet to the main channel and the sub-channel. Once the buffer flows through the sub-channel, air is passively trapped inside the predesigned cavity structure and the bubble is generated and stabilized at the desired position (Figure 1b). The next step is to load both the sample and buffer (PBS) from inlets. In this step, the culture chamber is closed to prevent the blood flow from entering the sub-channel and culture chamber, which is demonstrated in Figure 1c. The acoustic field is then turned on to selectively trap the CTCs on the bubble surface, which is located at the entrance of the sub-channel (Figure 1d). As aforementioned, the captured CTCs rotate and aggregate to a spheroid under the action of acoustic radiation force and drag force. When the spheroid grows to a desired size, the spiked blood sample flow is stopped, and the wash buffer is slowly infused until the sample is removed in the main channel to the outlet (Figure 1d). When the buffer flow stops, the CTC spheroid is then released into the culture chamber through the sub-channel by opening the culture chamber and turning off the acoustic field. During the CTC spheroid culture process, the culture chamber is closed to ensure the CTC culture media can be continuously supplied in the main channel. By fluid diffusion, the medium diffuses to the culture chamber without mechanical stress on CTCs (Figure 1e). By repeating step 3 (Figure 1d) and step 4 (Figure 1e) with controlling acoustic actuation and syringe pump, this platform can simply and rapidly create several CTC spheroids, which would be helpful for the tumor spheroid-based studies. It is also worth noting that to stop the device during the experiment, the first step is to stop the liquid flow by stopping the syringe pump and the second step is to turn off the acoustic actuation. Conversely, to restart the device, we need to turn on the acoustic actuation first and then start pumping the fluid into the main channel. This way the spheroid can remain to be trapped instead of flowing away. Additionally, the device has the capability to trap more CTC spheroids and culture them simultaneously by designing parallel sub-channels and culture chambers. Furthermore, by injecting anti-cancer drugs to the main channel, this ABSTRACT platform could be used to test the drug effect on the CTC spheroids.

3.2. Device design and optimization

To improve the CTCs trapping performance in the ABSTRACT platform, we optimized the platform design by systematically comparing several parameters with a set of experiments, including the geometry of the cavity structure, sample distance from the wall, flow rate of the spiked blood sample as well as input voltage on the piezoelectric transducer. These parameters are expected to impact the trapping efficiency.

3.2.1. Cavity geometry

Normally, a free-standing microbubble would keep a spherical shape by surface tension. When they are confined by the microcavity structures, they usually form a spherical cap or a hemicylindrical-shaped bubble. Under acoustic actuation, the target cells are trapped on one or two specific points of the bubble surface, which depends on the shape of the bubble. With the use of different geometries of cavity structure, the shape of the trapped bubble is distinct. Since the trapping location of CTCs depends on the shape of the bubble and the bubble shape can be determined by the geometry of the cavity structure, the cavity geometry is a critical parameter to determine the trapping location and the trapping efficiency of CTCs.

To identify the optimal trapping efficiency, we designed and tested five devices with different angled cavity structures (D1, D2, D3, D4, D5, θ = 90°, 120°, 45°, 30°, 135°). We first generated the air bubbles for the five devices by injecting the PBS into the main channel. Figure 3a shows the comparison of the shape of the five bubbles in different angled cavity structures. Spiked blood samples were then continuously injected into the devices at 2 μl/min and the acoustic field was turned on when the flow became stable. During the experiment, we observed that CTCs

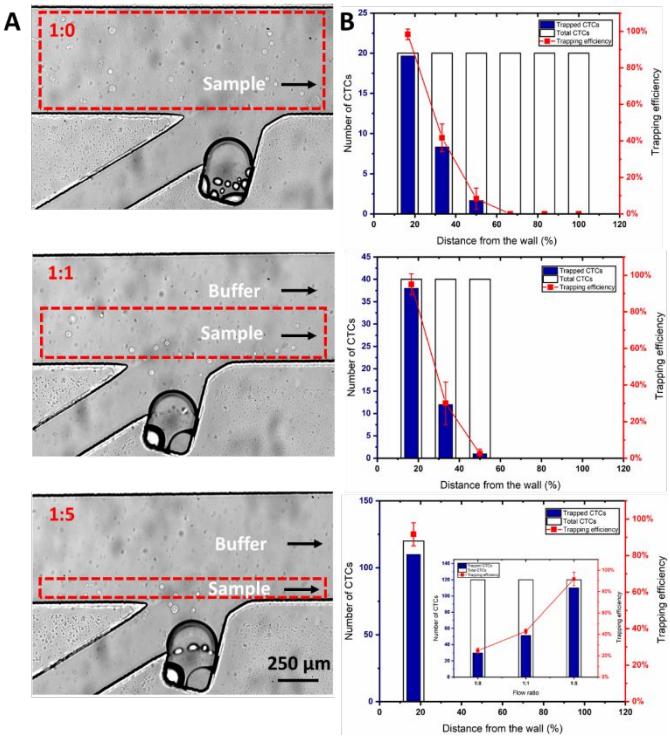

Figure 4. (a) Images of spiked blood samples in the main channel with different sheath flow ratios. (b) Plot of CTCs trapping efficiency at different sheath flow ratios (1:0, 1:1, 1:5). The data is presented as average ± standard deviation (n=3).

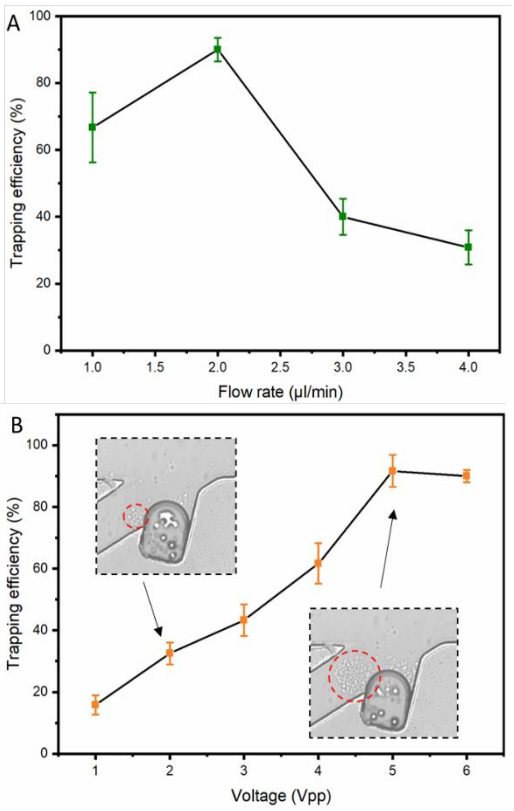

Figure 5. (a) CTCs trapping efficiency *versus* flow rates. (b) CTCs trapping efficiency *versus* input voltage. The data is presented as average ± standard deviation (n=3).

trapping locations were various for different shaped bubbles. If the trapping location was inside the sub-channel, the CTCs were trapped, rotated, and aggregated to form the spheroids. However, if the trapping location was in the main channel, the CTCs were trapped at first and then followed the streamline to the outlet. In the first situation, since the flow rate at this location was very low and can prevent CTCs from flowing away, the acoustic bubble captured more CTCs and CTCs were easily released to the culture chamber. For the second situation, the trapping efficiency became lower because CTCs experienced both microstreaming flow and laminar flow induced drag force. When the drag force was larger than the secondary radiation force, the trapped CTCs in the main channel flowed away with the bloodstream. To ensure the accuracy and repeatability, we repeat the experiment three times and measured the capture efficiencies for six regions separately. For each experiment, we tested 300 CTCs (50 CTCs for each region). After measuring and comparing the average trapping efficiency, we found D4 has the highest trapping efficiency among five devices (Figure 3), which is probably due to the fact that the trapping location is somewhat inside the sub-channel and CTCs are easier to be trapped because of the lower flow speed. In contrast, D3 and D5 have lower trapping efficiency since the trapping location is more in the main channel and the CTCs experienced a larger drag force than the secondary radiation force.

3.2.2 Distance from the wall

Theoretically, the magnitude of the secondary radiation force is strongly related to the distance between the bubble and the cell (Equation 2). Specifically, the largest secondary radiation force experienced by cells is estimated to be located at a fixed distance ($d \sim r_b + r$) away from the bubble surface.[32] With increasing the distance, the secondary radiation force decreases. This theoretical estimation is supportive of our experimental findings, which show that more CTCs are likely to be trapped when they close to the side of the wall where the bubble is located (lower wall). Therefore, we divided the channel (x-y plane) into six equal parts along the y-axis for measuring and comparing the trapping efficiency at different distances from the wall (Figure 3a). The measured result shows

that the trapping efficiency of CTCs decreases when the distance increases, which is presented in Figure 3 (b-f). Most of the CTCs in the closest region (w1) were trapped, while none of them were captured in the regions far away from the wall (w4, w5, w6).

3.2.3 Effect of sheath flow ratio

From the results of the previous section, we conclude that D4 (cavity geometry) and w1 region provides the best performance in trapping CTCs. However, the total trapping efficiency of CTCs in D4 is still relatively low due to distance limitations. To enhance the trapping efficiency, here we investigated the effect of different sheath flow ratios at the same total flow rate (2 µl/min). In the experiment, we injected sample and buffer sheath flow into inlets with the ratio of 1:0, 1:1 and 1:5 in D4, where the spiked blood sample is close to the lower wall. The samples in the main channel with different flow ratios are shown in figure 4a. Each experiment was repeated three times in the microfluidic device to ensure the data accuracy. For the flow ratio of 1:0, since the sample was distributed in the whole channel, we measured the sample in six regions (w1 to w6) separately; for the flow ratio of 1:1, the sample in w1, w2, w3 were measured since the sample flow was controlled in w1, w2, w3 region; for the flow ratio of 1:5, only in w1 was measured because the sample flow was controlled in w1 region. To make sure the results of these three flow ratios are comparable, the same total number of CTCs (120 cells) was set to be counted for each experiment. Figure 4b shows the result of trapping efficiency with respect to the sheath flow ratio. At the flow ratio of 1:5, the trapping efficiency reaches 92%, while the trapping efficiency is 43% and 25% at the 1:0 and 1:1 flow ratio, respectively. Therefore, we conclude that the trapping efficiency increases by increasing the sheath flow ratio. Figure 4b also illustrates the trapping efficiency in w1 regions reaches higher than 90% for all flow ratios, while the trapping efficiency dramatically decreases in other regions, which explains the reason why trapping efficiency increases when the sheath flow ratio decreases.

3.2.4 Effect of flow rate

From equation 1, the magnitude of drag force acts on cells increases when flow velocity increases. Therefore, the flow rate could influence the trapping efficiency of the CTCs. To experimentally investigate the flow rate effect on trapping efficiency, flow rate ranging from 1 to 4 µl/min was applied with the optimal sheath flow ratio of 1:5 and each experiment were repeated for three times. As shown in figure 5a, the results illustrate the trapping efficiency varies with the flow rate. The maximum trapping efficiency occurs when the flow rate is 2 µl/min and the secondary radiation force is dominant to trap more cells on the desired trapping location. From the experimental results, the distance of the cells and the bubble increases with decreasing the flow rate, which decreases the secondary radiation force based on the theory (Equation 2). Although the secondary radiation force is dominant, the decreasing force makes trapping efficiency lower. Therefore, at 1 µl/min, the trapping efficiency decreases. As the flow rate increases from 2 to 4 µl/min, the trapping efficiency decreases since the drag force gradually becomes larger and more cells follow the streamline to the outlet of the main channel.

3.2.5 Effect of input voltage

To further improve the trapping performance, we experimentally studied the effect of input voltage on trapping efficiency. We applied input voltages ranging from 1 to 6 Vpp with 1 Vpp increment to actuate the bubble trapped in D4. We conducted the experiment three times and the average capture efficiencies were calculated for different input voltages. Figure 5b shows that increasing the input voltage significantly improves the trapping efficiency from 1 to 5 Vpp, when the voltage increases from 5 Vpp to 6 Vpp, the trapping efficiency plateaued, and reaches the optimum value (~91%) in this device and to the threshold. This result shows a good agreement with the theoretical prediction, since the oscillation amplitude of the bubble increases with the input voltage, and thus the secondary radiation force becomes stronger to trap more CTCs into the desired trapping location (Equation 2).

3.3. CTC spheroid collection and culture

In the previous section, we introduce the principles of CTC spheroid formation and collection using the acoustic bubble (Figure 1). During the experiment, when the acoustic field was applied to generate microstreaming, the CTCs aggregated around the bubble surface and strong cell-cell connections were formed after ~30 min acoustic actuation (Figure 6a and 6b). The spheroids were then collected to the culture chambers via the sub-channels by opening the culture chambers. After spheroids moved to the culture chambers, we cultured them on the chip under sterile conditions at 37°C and 5% CO_2 for 3 days to demonstrate the culture ability of the ABSTRACT platform. After culturing for 1 hr, we observed that the boundary of the cells became blurred and started to disappear (Figure 6d). At this point, the fresh culture medium was injected into the inlet and diffused to the culture chamber. After culturing 36 hr, the surface of the spheroid became smooth and the spheroid compaction occurred, which was considered to be ready for drug testing or other spheroid-based experiments (Figure 6e).[33, 34]

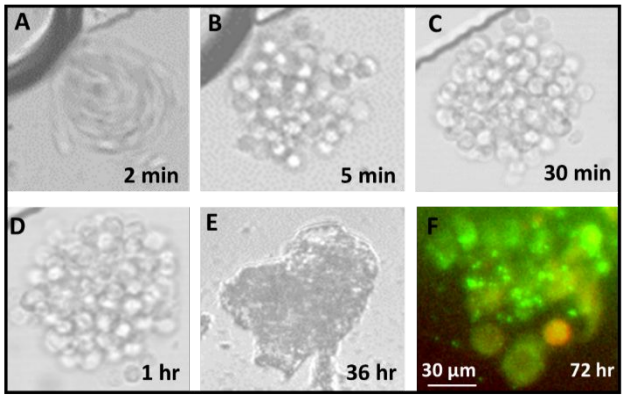

Figure 6. (a) CTCs trapped by acoustic bubbles in 2 min acoustic actuation. (b) CTCs aggregates after 5 min acoustic actuation. (c) After 30 min acoustic actuation, cell aggregates became larger and compact. (d) After culturing for 1 hr, cells began to form into spheroid and cell-cell boundary started to disappear. (e) After culturing for 36 hr, the surface of the spheroid became smooth. (f) Live/dead cell-staining images after 72 hr of spheroid culture. The cells were stained with Calcium-AM (green color – live cells) and BOBO-3 Iodide (orange color – dead cells)

To demonstrate the cell viability during the acoustic trapping and culture process, the live/dead cell assay was performed at the endpoint of spheroid culture (Figure 6f). The live cell and dead cell were labeled with Calcein, AM (green fluorescence) and BOBO-3 Iodide (orange fluorescence), respectively. To verify the viability testing results, we repeated three times for spheroid creation, collection and culture under the same condition. In each experiment, we created around 20 similar-sized spheroids and used 10 spheroids for the viability measurement each experiment. The result shows that the high cell viability (84%) was maintained after 3 days of culture. Based on the experimental results, our acoustic bubble-based Tumor-on-a-Chip platform demonstrates to be capable of forming and culturing viable CTC spheroids.

4. Conclusions

In summary, this acoustic bubble-based Tumor-on-a-Chip platform (ABSTRACT) has been shown to successfully trap and rotate CTCs, as well as form and culture CTC spheroids on a single chip without bulky lab equipment and complex operating procedures. In this study, by controlling the acoustic bubble, we demonstrate the ability of this platform to selectively capture CTCs from the continuous blood flow based on their physical properties. We also systematically explore the effect of geometry parameters, fluid parameters and input voltages on trapping CTCs to optimize the trapping efficiency of this platform. Moreover, we successfully show that the trapped CTCs can rapidly aggregate under acoustic actuation, as well as can release to the culture chamber to form the CTC spheroid through the sidewall sub-microchannel. More importantly, this platform has the capability to deliver culture medium to the CTC spheroids through the main channel by fluid diffusion for on-chip culture, which may be applied to test the drug effect on the CTC spheroids and contribute to developing personalized drug treatment in future.

Overall, the presented acoustic bubble-based Tumor-on-a-Chip platform provides a novel method to process CTCs on the chip. Compared with the conventional methods, this ABSTRACT platform enables multi-step CTCs processing on a chip (trapping, rotation and culture) in controllable and rapid manners. The simplicity of fabrication and experimental setup of this platform could reduce the cost and speed up the procedure for CTCs processing. In future, we believe this work has great potential to be applied in CTC downstream analysis and personalized medicine for cancer treatment.

Conflicts of interest

There are no conflicts to declare.

Acknowledgements

This work was supported by NASA Early Career Faculty grant (80NSSC17K0522) and National Science Foundation grant (1917295). Yuan Gao and Qiyue Luan thank the support from the Graduate Research/Deiss Award in Biomedical Graduate Research from UIC.

References

1 E. M. Ferlay J, Lam F, Colombet M, Mery L, Piñeros M, Znaor A, Soerjomataram I, Bray F, Global Cancer Observatory: Cancer Today. Lyon, France: International Agency for Research on Cancer. , https://gco.iarc.fr/today, (accessed July 10, 2021).
2 J. Massagué and A. C. Obenauf, *Nature*, 2016, **529**, 298-306.
3 K. Pantel, C. Alix-Panabières and S. Riethdorf, *Nature reviews Clinical oncology*, 2009, **6**, 339-351.
4 W. S. Low and W. A. B. Wan Abas, *BioMed research international*, 2015, **2015**.
5 P. Li, Z. S. Stratton, M. Dao, J. Ritz and T. J. Huang, *Lab on a Chip*, 2013, **13**, 602-609.
6 J. Zhou, P. Mukherjee, H. Gao, Q. Luan and I. Papautsky, *APL bioengineering*, 2019, **3**, 041504.
7 J. Zhou and I. Papautsky, *Microsystems & Nanoengineering*, 2020, **6**, 1-24.
8 J. M. Martel and M. Toner, *Annu. Rev. Biomed. Eng.*, 2014, **16**, 371-396.
9 J. Zhang, S. Yan, D. Yuan, G. Alici, N.-T. Nguyen, M. E. Warkiani and W. Li, *Lab on a Chip*, 2016, **16**, 10-34.
10 A. Mishra, T. D. Dubash, J. F. Edd, M. K. Jewett, S. G. Garre, N. M. Karabacak, D. C. Rabe, B. R. Mutlu, J. R. Walsh and R. Kapur, *Proceedings of the National Academy of Sciences*, 2020, **117**, 16839-16847.
11 H.-S. Moon, K. Kwon, S.-I. Kim, H. Han, J. Sohn, S. Lee and H.-I. Jung, *Lab on a Chip*, 2011, **11**, 1118-1125.
12 M. Antfolk, S. H. Kim, S. Koizumi, T. Fujii and T. Laurell, *Scientific reports*, 2017, **7**, 1-12.
13 M. Wu, P. H. Huang, R. Zhang, Z. Mao, C. Chen, G. Kemeny, P. Li, A. V. Lee, R. Gyanchandani and A. J. Armstrong, *Small*, 2018, **14**, 1801131.
14 N. Garg, T. M. Westerhof, V. Liu, R. Liu, E. L. Nelson and A. P. Lee, *Microsystems & Nanoengineering*, 2018, **4**, 1-9.
15 S. Sharma, R. Zhuang, M. Long, M. Pavlovic, Y. Kang, A. Ilyas and W. Asghar, *Biotechnol. Adv.*, 2018, **36**, 1063-1078.
16 A. Hashmi, G. Yu, M. Reilly-Collette, G. Heiman and J. Xu, *Lab on a Chip*, 2012, **12**, 4216-4227.
17 Y. Gao, M. Wu, Y. Lin and J. Xu, *Lab on a Chip*, 2020, **20**, 4512-4527.
18 A. R. Tovar, M. V. Patel and A. P. Lee, *Microfluidics and Nanofluidics*, 2011, **10**, 1269-1278.
19 Y. Gao, M. Wu, Y. Lin, W. Zhao and J. Xu, *Microfluidics and Nanofluidics*, 2020, **24**, 1-10.
20 D. Ahmed, X. Mao, J. Shi, B. K. Juluri and T. J. Huang, *Lab on a Chip*, 2009, **9**, 2738-2741.
21 Y. Lin, C. Gao, Y. Gao, M. Wu, A. A. Yazdi and J. Xu, *Sensors and Actuators B: Chemical*, 2019, **287**, 312-319.
22 M. V. Patel, A. R. Tovar and A. P. Lee, *Lab on a Chip*, 2012, **12**, 139-145.
23 M. V. Patel, I. A. Nanayakkara, M. G. Simon and A. P. Lee, *Lab on a Chip*, 2014, **14**, 3860-3872.
24 P. Marmottant and S. Hilgenfeldt, *Proceedings of the National Academy of Sciences*, 2004, **101**, 9523-9527.
25 Y. Chen, Z. Fang, B. Merritt, D. Strack, J. Xu and S. Lee, *Lab on a Chip*, 2016, **16**, 3024-3032.

26 D. Ahmed, A. Ozcelik, N. Bojanala, N. Nama, A. Upadhyay, Y. Chen, W. Hanna-Rose and T. J. Huang, *Nat. Commun.*, 2016, **7**, 1-11.

27 Y. Xu, A. Hashmi, G. Yu, X. Lu, H.-J. Kwon, X. Chen and J. Xu, *Appl. Phys. Lett.*, 2013, **102**, 023702.

28 A. R. Tovar and A. P. Lee, *Lab on a Chip*, 2009, **9**, 41-43.

29 P. B. Muller, R. Barnkob, M. J. H. Jensen and H. Bruus, *Lab on a Chip*, 2012, **12**, 4617-4627.

30 W. T. Coakley and W. Nyborg, *Ultrasound: Its applications in medicine and biology*, 1978, **3**, 77-159.

31 W. Qiu, J. T. Karlsen, H. Bruus and P. Augustsson, *Physical Review Applied*, 2019, **11**, 024018.

32 P. Rogers and A. Neild, *Lab on a Chip*, 2011, **11**, 3710-3715.

33 K. Chen, M. Wu, F. Guo, P. Li, C. Y. Chan, Z. Mao, S. Li, L. Ren, R. Zhang and T. J. Huang, *Lab on a Chip*, 2016, **16**, 2636-2643.

34 K. Kwapiszewska, A. Michalczuk, M. Rybka, R. Kwapiszewski and Z. Brzózka, *Lab on a Chip*, 2014, **14**, 2096-2104.